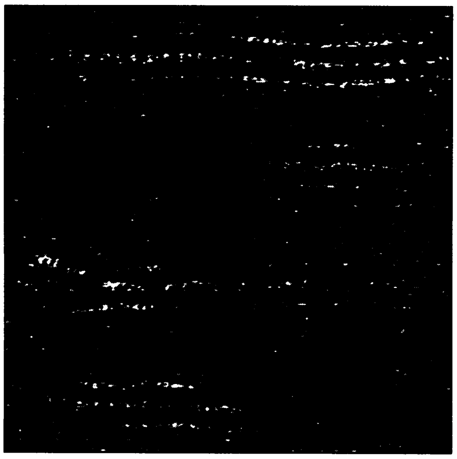

Fig. 4. An example of the localized structures for $\sigma = 0.6 \times 10^{-8}$ ohm^{-1} m^{-1} and $\varepsilon = 0.05$. The image covers an area of 0.17 cm by 0.17 cm.

ulated, yielding an amplitude that varied only slightly over the image. The spatial average $A_n(t)$ was then studied separately for the four modes. A 30-min segment of $A_n(t)$ for the right-traveling zig and zag rolls for $\varepsilon = 0.01$ is shown in Fig. 3. At times one of the modes dominates, and at other times the modes have approximately equal amplitudes. Computation of the cross-correlation of pairs of the $A_n(t)$ from a 4-hour time series showed that the four modes are anticorrelated with each other. The autocorrelation time of a single $A_n(t)$ was roughly $1000\tau_d$ for all four modes [where $\tau_d = \mathcal{O}(1\ \text{s})$ is the director relaxation time]. This state persisted for the duration of the experiment (>48 hours).

Qualitatively different chaotic phenomena occur in this system when σ is small. For $\sigma = 0.6 \times 10^{-8}$ ohm^{-1} m^{-1}, we observed no evidence of any spatially extended STC. Instead, highly localized elongated convective structures or pulses, consisting of traveling waves under a slowly moving envelope, coexisted with regions of pure conduction up to $\varepsilon \approx 0.1$. Because of their spatial and temporal appearance, we refer to these pulses as "worms." An example is shown in Fig. 4 for $\varepsilon = 0.05$. In the direction perpendicular to $\hat{n}$, the worms had a unique width equal to a few times λ. Parallel to $\hat{n}$, they had a distribution of lengths.

An exciting prospect for the future is to compare quantitative, experimentally determined statistical measures of these states with calculations based on the equations of motion of this system. Calculations based on weakly nonlinear theory should be possible because the experiment (see Fig. 2) indicates that the mean-square amplitudes of the chaotic states grow continuously from 0 as the system is driven further from equilibrium and because only a small number of modes is involved in the spatiotemporal complexity. Such a comparison may yield useful insights into the nature of STC. It remains to be seen to what extent the lessons learned from this specific system can be applied to STC in general.

REFERENCES AND NOTES

1. M. C. Cross and P. C. Hohenberg, *Rev. Mod. Phys.* **65**, 851 (1993); *Science* **263**, 1569 (1994).
2. G. Ahlers, *Phys. Rev. Lett.* **33**, 1185 (1974); J. P. Gollub and H. L. Swinney, *ibid.* **35**, 927 (1975).
3. M. Treiber and L. Kramer, *Mol. Cryst. Liq. Cryst.* **261**, 311 (1995).
4. Another system in which STC evolves from the uniform state by means of a supercritical bifurcation is convection in an isotropic fluid with rotation about a vertical axis [G. Küppers and D. Lortz, *J. Fluid Mech.* **35**, 609 (1969)]. However, in this case it is not clear that the system can be described by a small number of modes and the corresponding coupled Ginzburg-Landau equations. Attempts to do so have led to disagreement with experimental results [Y. Hu, R. E. Ecke, G. Ahlers, *Phys. Rev. Lett.* **74**, 5040 (1995) and references therein].
5. For a recent review of pattern formation in liquid crystals, see L. Kramer and W. Pesch, *Annu. Rev. Fluid Mech.* **27**, 515 (1995).
6. M. Dennin, M. Treiber, L. Kramer, G. Ahlers, D. S. Cannell, *Phys. Rev. Lett.* **76**, 319 (1996).
7. M. Dennin, G. Ahlers, D. S. Cannell, in *Spatio-Temporal Patterns*, P. E. Cladis and P. Muhoray, Eds. (Addison-Wesley, Reading, MA, 1994), pp. 353–365.

8. Supported by NSF grant DMR94-19168.

23 October 1995; accepted 16 February 1996

Continental Crust, Crustal Underplating, and Low-*Q* Upper Mantle Beneath an Oceanic Island Arc

Kiyoshi Suyehiro,* Narumi Takahashi, Yoshiro Ariie, Yasutaka Yokoi, Ryota Hino, Masanao Shinohara, Toshihiko Kanazawa, Naoshi Hirata, Hidekazu Tokuyama, Asahiko Taira

A detailed structural model of the crust, subducting slab, and underlying upper mantle across the northern Izu-Ogasawara (Bonin) island arc system is derived from a marine seismic reflection and ocean bottom seismographic refraction survey and subsequent forward modeling combined with tomographic inversion. The model indicates that the crust is thickest beneath the presently active rift zone and a granitic crust may have formed in the mid-crust. A highly attenuative mantle (that is, one with low quality *Q*) seems to be confined mainly beneath the presently active rift zone. In contrast, high *P*-wave velocity persists in the lower crust between the forearc and eastern margin of the back arc basin, suggesting a large-scale magma input responsible for the arc formation.

Oceanic island arcs (OIAs) develop at oceanic plate boundaries, where one plate is subducted below the other. The subduction produces intense igneous activity below the overriding plate, leading to the formation of a volcanic arc. Eventually, the volcanic arc may accrete to a continent and become a component of the continental crust. This connection to the continental crust has led some workers to suggest that continental crust formation began at OIAs in the early history of the Earth (*1*). In addition, the mechanisms of subduction, melt initiation, slab dehydration, and arc volcanism at OIAs are poorly understood. Modeling the seismic structure of the OIA crust, in order to constrain the volume and type of crustal accretion and its composition, particularly in the deeper crust, of which very little is known, is essential to understanding OIA evolution and its role in the growth of continental crust.

The Izu-Ogasawara arc system located off the southern coast of Japan, extending more than 1000 km from north to south, is a site of active rifting and subduction (Fig. 1) (*2, 3*). The arc formation was probably initiated at an intraoceanic transform fracture zone boundary about 48 million years ago (Ma) (*4*). The initial arc volcanism, characterized by tholeiite and boninite lavas, created an arc 300 to 450 km wide. Rifting during the Oligocene formed the forearc and back arc basins, which resulted in the spreading of the Shikoku Basin (until 15 Ma) and the separation of Kyushu-Palau Ridge. The arc volcanism revived about 17 Ma and intensified about 2 Ma, creating the present-day volcanic front (VF), including occasional forearc volcanic intrusions and chains of volcanoes that obliquely cross the

K. Suyehiro, N. Takahashi, Y. Ariie, Y. Yokoi, H. Tokuyama, A. Taira, Ocean Research Institute, University of Tokyo, Tokyo 164, Japan.
R. Hino, Faculty of Science, Tohoku University, Sendai 981, Japan.
M. Shinohara, Department of Earth Sciences, Chiba University, Chiba 263, Japan.
T. Kanazawa and N. Hirata, Earthquake Research Institute, University of Tokyo, Tokyo 113, Japan.

*To whom correspondence should be addressed.

back arc (*3*). Current rifting, which started about 2 Ma, has produced a series of monogenetic volcanoes in the rift basins (*5*) within north-south–trending normal faults in a zone about 70 km wide (*6*).

The forearc contains an along-arc chain of serpentinite seamounts inferred to result from mantle diapirs formed by the release of water from the subducted oceanic crust. The Pacific Plate has been estimated to subduct at an angle of 22° down to a depth of 60 km and to extend to a depth of 120 km beneath the VF (*7*), which is about the depth of the amphibole-chlorite decomposition-dehydration boundary (*8*).

We conducted an extensive seismic reflection and refraction survey in 1992 across the northern Izu-Ogasawara island arc system at 32°15′N between 138° and 143°E, transecting the entire OIA system (Fig. 1) (*9*). Controlled sources and natural earthquakes were used to model the two-dimensional (2D) crustal and uppermost mantle structure and subduction slab geometry. Forward modeling of the controlled-source seismic data gave us a detailed model of the *P*-wave velocity structure across the entire arc (Fig. 2) (*10, 11*). A simultaneous inversion of the airgun data of one east-west and two north-south profiles obtained by seven ocean-bottom seismometers (OBSs) in the rift basin (Fig. 1) confirmed the complex upper crustal structure of the rift zone (*12, 13*). We found that (i) the crust is thickest (~20 km) beneath the presently active rift zone, (ii) the middle crust confined beneath the arc has a velocity of ~6 km/s, extending as far east as the VF and comprising about 25% of the crustal volume, (iii) the lower crust has a velocity ranging between 7.1 and 7.3 km/s, occupying more than 30% of the total crust, (iv) the Mohorovičić discontinuity (Moho) becomes obscure east of the VF, (v) in the rift zone, lateral velocity variation is large, and high velocity conduit-like features can be seen, (vi) a low-velocity zone in the upper crust is located about 10 km east of the eastern margin uplift of the Aoga Shima rift and extends down to the middle crust, (vii) extremely low velocity is observed beneath the forearc serpentinite diapir, and (viii) the crust at the eastern margin of Shikoku Basin is thicker than normal oceanic crust, and the lower crust is faster, exceeding 7 km/s.

The attenuation of seismic wave amplitudes is a good indicator of anelastic characteristics of the crust and mantle. We mapped attenuative zones on the basis of relative amplitudes and the predominant frequencies (~5 to 15 Hz) of seismic waves from deep and shallow earthquakes at different OBS stations and found that (i) the predominant frequencies from shallow events are similar on both sides of the arc, (ii) events deeper than 300 km are unobservable at OBSs in the rift zone, and (iii) along-arc ray paths are attenuated throughout the rift zone (Fig. 3) (*14, 15*). Although these observations are insufficient to give a unique model, they can be explained if the attenuation is restricted between the VF and the Nishi-Shichito Ridge in the crust and upper mantle above the subducted plate (Fig. 4).

The relatively low velocity (~6 km/s) and its small increase with depth in the middle crust beneath the arc might be attributable to granitic rocks. Although the low *P*-wave velocities alone are not conclusive regarding exact composition, they are consistent with a composition of tonalite. In addition, tonalite was dredged from the Kyushu-Palau Ridge (*16*), which is believed to have rifted from the Izu-Ogasawara arc during the opening of the Shikoku Basin. An independent seismic survey has shown that the crust has seis-

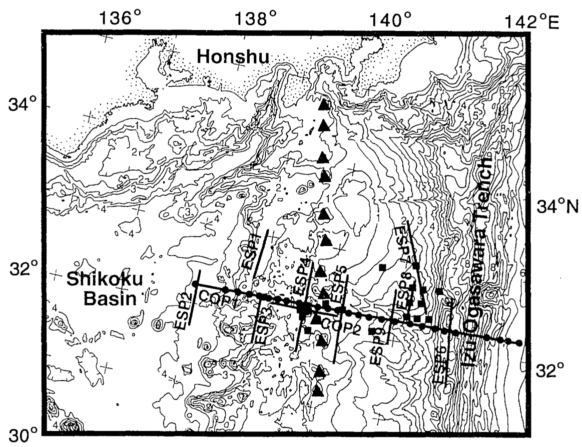

Fig. 1. Bathymetry of the Izu-Ogasawara oceanic island arc and its vicinity. The contours show the depths of the ocean floor in 0.5-km intervals. The numbers indicate depths in kilometers. Symbols: (▲) active volcanoes along the volcanic front; (●) OBSs used for the main profile; (■) OBSs used for the ESP and COP (*9*).

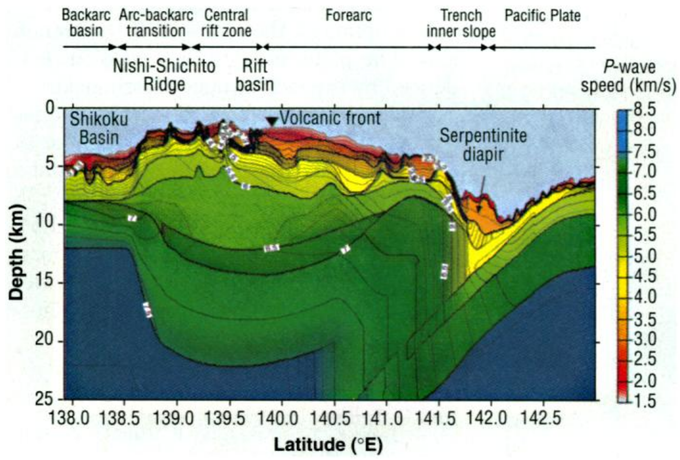

Fig. 2. *P*-wave velocity distribution across the Izu-Ogasawara arc along 32°15′N. Contours represent lines of constant velocity and the contour interval is 0.1 km/s. Contours are labeled every 0.5 km/s with thicker lines. Velocity discontinuities cause contour overlaps. The velocities are also color coded.

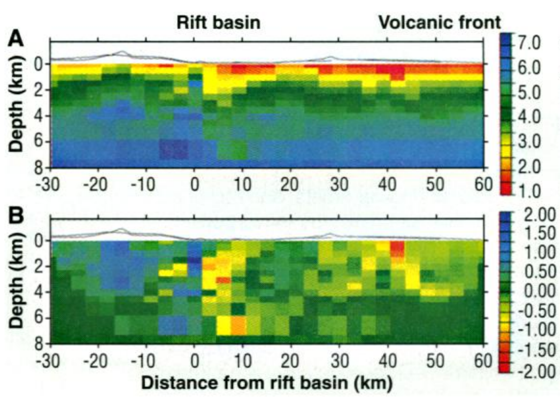

Fig. 3. (**A**) Upper crustal structure from inverse modeling (*13*). The distance origin is at 139.63°E (ESP4 longitude) (Fig. 1) at the deepest but western portion of the Aoga Shima rift basin (between −15 and 28 km on axis). Two topography lines above model datum correspond to those along the main profile and COP2. The initial model of the *P*-wave velocity structure starts from 2.0 km/s at the datum, smoothly increasing to 5.0 km/s at a depth of 3.1 km and 6.5 km/s at a depth of 14.2 km. The final model after five iterations is shown. (**B**) Distribution of *P*-wave velocity anomaly. Velocity deviations are differences from 1D model obtained by averaging the 2D model in (A).

mic velocities of 6 km/s beneath the Kyushu-Palau Ridge (*17*). Second, tonalite complex is exposed north of the Izu Peninsula, as a result of the collision of the northern end of the Izu-Ogasawara arc with the Honshu arc (*18*). This complex can be correlated with the middle crust of the present Izu-Ogasawara arc. The presence of gabbro or metagabbro in the Izu-Ogasawara arc would require anomalously

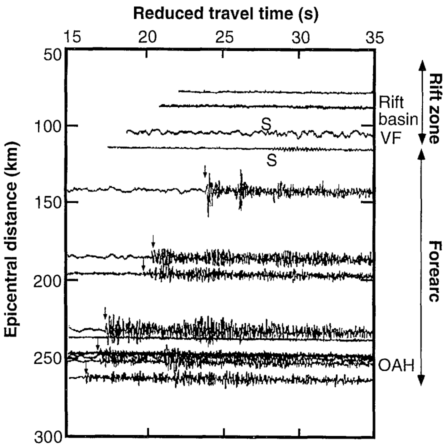

Fig. 4. Seismograms (vertical component) from a deep event (33.24°N, 138.79°E, 310-km depth) observed across the arc. The OBSs in the rift basin only registered low frequencies at low signal-to-noise ratios (*P*-wavetrain marked S), in contrast to high-frequency clear arrivals at OBS stations in the forearc and eastward (*P* onsets shown by arrows). Travel time is reduced by 8 km/s. VF is the volcanic front; OAH is the outer-arc high wall.

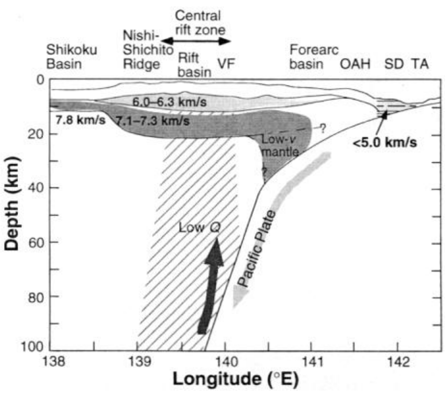

Fig. 5. Schematic cross section through northern Izu-Ogasawara arc, based on our models. Thin lines indicate structural boundaries (topography; upper, middle, and lower crusts; and top of subducting slab). Slab geometry is inferred from Fig. 2 and deep seismicity (*9*). Broken lines show where structural boundaries are not clear. Characteristic *P*-wave velocities of the arc system are indicated by shaded tones. See Fig. 2 for complete velocity distribution at crustal depths. Hypothetical magma path within low-*Q* zone (hatched zone) inferred from attenuation of seismic waves is shown in the upper mantle. SD is the serpentinite diapiric seamount; TA is the trench axis.

high temperatures or abundant fractures over a large area to explain our observations (*19*), neither of which are probable because of the observed heat flow over the rift (*20*) and the high overburden pressure at this depth, respectively.

The crustal models obtained at 31° and 33.5°N from previous investigations, although less constrained at greater depths, show similar features at the rift zone and along the forearc basin (*21*), suggesting that the basic arc structure continues along the arc. Thus, we estimate that on the order of 500 km^3 of granitic crust may be produced for every kilometer of arc in an OIA setting, which indicates a growth rate of ~10 to 25 km^3 per kilometer per million years, depending on the formation time length of 20 to 47 million years.

Conduit-like features in the rift basin of velocity higher than that of the surrounding upper crust (Fig. 2) may be caused by dike swarms that feed the monogenetic volcanoes through volcaniclastic sediments and lava flows that compose the rift basin upper crust. That the middle and lower crusts are thickest below the central rift zone indicates that there must be an additional igneous input to overcome tectonic thinning. Further below, the low-*Q* zone down to the slab is the likely region where melt is initiated.

Finally, we note implications on the seismic coupling of the plates near the trench axis. The plate interaction is weak, as evidenced by the lack of major earthquakes or accretionary prisms (*22*). The lack of activity may be explained by the existence of low-velocity material that persists without a clearly defined Moho to about 140.5°E above the subducting crust (Figs. 2 and 5). Continuous water release from the subducting slab may reduce the velocities of lower crustal rocks and mantle peridotites, causing weak interplate coupling.

REFERENCES AND NOTES

1. A. Taira, K. T. Pickering, B. F. Windley, W. Soh, *Tectonics* **11**, 1224 (1992).
2. E. Honza and K. Tamaki, in *The Ocean Basins and Margins*, A. E. M. Nairn, F. G. Stehli, S. Uyeda, Eds. (Plenum, New York, 1985), vol. 7A, chap. 10.
3. B. Taylor, in *Proceedings of the Ocean Drilling Program: Scientific Results* (Ocean Drilling Program, College Station, TX, 1992), vol. 126, pp. 627–651.
4. S. Uyeda and Z. Ben-Avraham, *Nature* **240**, 176 (1972).
5. A. Klaus, B. Taylor, G. F. Moore, F. Murakami, Y. Okamura, *Island Arc* **1**, 16 (1992).
6. S. Morita, thesis, University of Tokyo (1994).
7. R. Jarrard, *Rev. Geophys.* **24**, 217 (1986); B. L. Isacks and M. Barazangi, in *Island Arcs Deep Sea Trenches and Back-Arc Basins*, M. Talwani and W. C. Pitman III, Eds. (American Geophysical Union, Washington, DC, 1977), pp. 99–114.
8. Y. Tatsumi, *Geophys. Res. Lett.* **13**, 717 (1986).
9. The marine seismological survey used controlled sources and local earthquakes to model the crust, upper mantle, and subducting slab. Seismic reflection profiles—consisting of nine two-ship expanding spread profiles (ESP) along strike of the arc, two two-ship constant-offset profiles (COP), and the main profile of the whole transect—were shot with an airgun array (17 to 60 liters) and received by a 24-channel hydrophone streamer. Along-strike profiles were selected to sample the forearc, rift zone, and back arc. A total of 46 OBSs were laid out 15 to 20 km apart to receive airgun and dynamite shots along these profiles, in order to sample deep structure with wide-angle reflections and refractions. Two OBS seismic arrays were effectively configured to determine local shallow and deep seismicity across the arc, particularly beneath the forearc and rift zone (Fig. 1).
10. N. Takahashi, thesis, Chiba University (1995).
11. Detailed water depths and acoustic basements were constrained by multichannel seismic reflection profiling. Along-arc record sections of ESP and OBS profiles were inverted in the intercept time-ray parameter space to 1D velocity-depth models for each profile. On the basis of these constraints, a 2D ray-tracing forward modeling was performed for the across-arc profile to obtain a model that fit all of the picked arrivals in OBS record sections within 0.1 s of the observed value and explains the amplitude changes of these seismic phases with distance. The observed across-arc ray paths—interpreted to be *P*, *PmP*, *Pn*, and intracrustal wide-angle reflection phases—cover the entire arc down to depths of about 30 km. Because of the large OBS spacing and the lack of dynamite shots across the trench axis, the modeling of the structure at about 142°E (about 30 km wide above a depth of 15 km) relied chiefly on constraints from ESP6 (Fig. 1) record.
12. Y. Ariie, thesis, University of Tokyo (1994).
13. The inversion scheme allows 3D ray paths through 2D structures modeled by linearly varying velocities where velocities are assigned at nodes of 1906 points of 3630 triangles, each with 1.5-km horizontal and 0.25-km (depth, 1.7 to 5 km) or 0.75-km (depth, 5 to 12.5 km) distances (*23*). A datum line was defined at a depth of 1.7 km. Corrections for travel times above this depth were made using reflection seismic data, taking ray paths into consideration. Travel times for *P* waves from three independent profiles (COP2, ESP4, and main profile) were simultaneously inverted using 4672 ray paths. Five iterations were made to converge to the model shown in Fig. 3.
14. Y. Yokoi, thesis, Chiba University (1994).
15. The earthquake locations were made from the two OBS arrays (squares in Fig. 1). Out of 453 local earthquakes determined between 27 May and 11 June 1992, 20 representative events that occurred at crustal depths and in the subducting slab down to 372 km were used to geometrically constrain the attenuative zones. The OBS sensors are equipped with 4.5-Hz velocity sensors, which are not adequate to quantitatively estimate upper mantle *Q*. However, relative comparisons among different station-source pairs made it possible to map attenuative paths at a higher spatial resolution than previously available.
16. H. Tokuyama, H. Kagami, N. Nasu, *Bull. Ocean Res. Inst. Univ. Tokyo* **22**, 1 (1986).
17. M. Hayashida *et al.*, *Technical Bulletin of Hydrography* (Hydrographic Department of Japan, Tokyo, 1989), vol. 7, p. 25.
18. T. Matsuda, *J. Phys. Earth* **26**, S409 (1978); N. Niitsuma and F. Akiba, in *Formation of Active Ocean Margins*, N. Nasu, K. Kobayashi, S. Uyeda, I. Kushiro, H. Kagami, Eds. (Terrapub, Tokyo, 1985), pp. 75–108; K. Sato, *Mod. Geol.* **15**, 367 (1991).
19. M. H. Salisbury and N. I. Christensen, *J. Geophys. Res.* **83**, 805 (1978); N. I. Christensen and J. D. Smewing, *ibid.* **86**, 2545 (1981).
20. T. Yamazaki, *Bull. Geol. Surv. Jpn.* **43**, 207 (1992).
21. R. Hino, thesis, Tohoku University (1991).
22. H. Kanamori, *Tectonophysics* **12**, 187 (1971); S. Uyeda and H. Kanamori, *J. Geophys. Res.* **84**, 1049 (1979).
23. D. Caress, M. S. Burnett, J. A. Orcutt, *J. Geophys. Res.* **97**, 9243 (1992).

24. We thank two anonymous reviewers for critically reading the manuscript.

10 August 1995; accepted 5 February 1996